Submitted to ADVANCED MATERIALS
DOI: 10.1002/adma.((please add manuscript number))

Metal organic covalent network chemical vapor deposition for gas separation

By *Nicolas D. Boscher*,† *Minghui Wang*,† *Alberto Perrotta*, *Katja Heinze*, *Mariadriana Creatore* and *Karen K. Gleason**

†These authors contributed equally to this work.

Dr. N. D. Boscher, Dr. M. Wang, Prof. K. K. Gleason
Department of Chemical Engineering
Massachusetts Institute of Technology
77 Massachusetts Avenue, Cambridge, Massachusetts 02139 (United States)
E-mail: kkg@mit.edu
Dr. N. D. Boscher
Department of Materials Research and Technology
Luxembourg Institute of Science and Technology
5 Avenue des Hauts-Fourneaux, Esch/Alzette, L-4362 (Luxembourg)
A. Perrotta, Prof. M. Creatore
Department of Applied Physics
Eindhoven University of Technology
5600 MB Eindhoven (The Netherlands)
Prof. Dr. K. Heinze
Institute of Inorganic and Analytical Chemistry
Johannes Gutenberg University of Mainz
Duesbergweg 10-14, D-55128 Mainz (Germany)

Keywords: Metalloporphyrins; iPECVD; Free-radical polymerization; Metal organic covalent network; Gas separation

Membrane gas separation is an energy efficient and environmentally friendly technology when compared to conventional cryogenic distillation or adsorption processes.[1] Important gas pairs separated by membrane processes include H_2/N_2 or H_2/CH_4 for H_2 recovery, O_2/N_2 for O_2 and N_2 enrichment, CO_2/CH_4 for pre-combustion natural gas sweetening and CO_2/N_2 for post-combustion CO_2 capture.[2] To achieve high flux, one key strategy is to fabricate ultra-thin gas selective layers, since the flux is inversely proportional to the thickness of a membrane.[3] In this regard, good H_2/CO_2 separation performances were reported for porous alumina supported metal organic framework

(MOF) nanosheets and graphene oxides (GOs) atomic sheets.[4,5] However, such membranes can only be prepared over small lateral dimensions and remain extremely brittle. Thus, they can only operate at zero transmembrane pressure difference, which seriously restrains their practical applications. Porous silicon nitride (SiN_x) framework supported porous graphene films with superior mechanical sturdiness were fabricated by focused ion beam (FIB) perforation, but the relative large pores only afford very low gas selectivities.[6] In contrast, polymer membrane supported graphene and GOs films showed better gas selectivities, although low gas permeances (*i.e.* pressure normalized gas flux) for the coated polymer membranes were observed.[7] To minimize the permeance loss while maximizing the gas selectivities, Sivaniah E. *et al.*,[8,9] introduced controlled oxidative surface modification methods (*e.g.* photo-oxidative and thermal oxidative) to optimize the gas separation performances of PIM-1, an intrinsic microporous polymer having a nominal pore size < 2 nm. The resulting membranes showed enhanced gas selectivities while maintaining high gas permeabilities. However, such methods are highly substrate dependent.

Porphyrins and porphyrin derivatives are robust and versatile functional molecules since their properties can be tuned through the choice of both their central metal ion and peripheral and axial substituents.[10–12] Their rigidity and chemical stability make them ideal as building units for the formation of covalent organic frameworks (COFs) and coordination metal-organic frameworks (MOFs) by wet chemistry approaches.[13] In particular, the narrow distribution of the micropore structures within porphyrin polymers has proved to be useful for gas sensing, storage and separation.[14] However, it is of great

difficulty to produce large and hyper-thin (*i.e.*, less than 100 nm) gas selective porphyrin-based layers by conventional wet chemistry methods.[15] Exploiting the fact that porphyrins possess free-radical polymerizable bonds,[16,17] we explored for the first time the polymerization of metalloporphyrins via an up-scalable, substrate independent and fast iPECVD approach, which resulted in the formation of a new type of hyper-thin metal organic covalent network (MOCN).[18] In contrast to the previously described materials, the iPECVD MOCN was fabricated in a single step directly on its support over significant area (*i.e.* 175 cm^2) to yield a flexible supported membrane. The gas transport properties of the resulting novel hyper-thin and pinhole-free porphyrin-based MOCN films were further assessed, including operation at high transmembrane pressure differences (*e.g.* 10 bar), in order to evaluate the potential of this approach for membrane gas separation.

To illustrate our CVD approach, we selected the commercially available zinc (II) *meso*-tetraphenylporphyrin (ZnTPP) (**Figure 1**a). Our strategy relies on the radical polymerizability of one exo-pyrrole double bond of the porphyrin rings.[16,17] A low power (*ca.* 20 W) capacitively coupled radio-frequency (RF) plasma discharge (Figure 1c and Figure S1, Supporting Information) avoids decomposing the robust porphyrin while selectively cleaving the labile initiator, *i.e. tert*-butyl peroxide (TBPO), to form radicals. The free radical polymerization produces a highly visible color change. Whereas evaporated ZnTPP is reddish, the MOCN coating is green, as shown in Figure 1d. UV-vis absorption spectroscopy (Figure 1e) confirmed that one of the *exo*-pyrrole double bonds of ZnTPP is reduced (Figure 1a), resulting in the appearance of three new absorption

bands, at 510 nm, 602 nm and 626 nm, assigned to the $Q_x(0,1)$, $Q_y(0,1)$ and $Q_y(0,0)$ transitions of zinc (II) *meso*-tetraphenylchlorin (ZnTPC) (Figure 1b). The strong decrease of the band intensity located at 555 nm corresponds to the $Q_y(0,0)$ transition of ZnTPP.[19] No evidence of further reduction of the other available *exo*-pyrrole double bonds of the porphyrinoid ring could be detected. Nevertheless, if the characteristic absorption band of zinc (II) *meso*-tetraphenylbacteriochlorin (ZnTPBC) above 700 nm is not observed, the formation of zinc (II) *meso*-tetraphenylisobacteriochlorin (ZnTPiBC) cannot be excluded due to a possible overlap of its absorption bands with the strong ones of ZnTPP and ZnTPC (Figure 1e).[20]

The intensity of the strong absorption band located around 430 nm originated from the Soret bands of ZnTPP and/or ZnTPC is almost identical for the evaporated ZnTPP and the MOCN coating. This indicates the excellent selectivity of the chosen iPECVD approach, which allows retaining the 18 π e^- conjugation of the porphyrinoid while efficiently ensuring its polymerisation and conversion of the ZnTPP to ZnTPC. Indeed, the rather soft RF plasma discharge employed is expected to easily cleave the peroxide initiator, *i.e.* TBPO, that will further provide well defined radicals and induce a highly selective reactivity.[18] In addition to the observations related to the absorption intensities, the position of Soret bands can also provide information on the environment of the porphyrinoids. Despite the fact that the ZnTPC Soret band absorbs at longer wavelengths (*i.e.* 420 nm in *n*-hexane solution) than the Soret band of ZnTPP (*i.e.* 414 nm in *n*-hexane solution),[21,22] the position of the Soret band of the MOCN coating is observed at a significantly shorter wavelength (*i.e.* 427 nm) than the evaporated ZnTPP (*i.e.* 437 nm)

(Figure 1e). This 10 nm hypsochromic shift, which may also be slightly induced by the presence of new *beta*-substituents to the ZnTPC formed during the iPECVD process,[23] is indicative of a reduced stacking of the porphynoids. Indeed, the strong bathochromic shift (*i.e.* $\Delta\lambda$ = 23 nm) between the Soret band of the evaporated ZnTPP (*i.e.* 437 nm) and the one of ZnTPP in *n*-hexane solution (*i.e.* 414 nm) is indicative of a J-type aggregation of the porpyhrins, *i.e.* pi-pi stacking driven by non-covalent interactions.[24,25] If polymerized into a ZnTPC covalent network, pi-pi stacking is likely to be prevented and a far less pronounced bathochromic shift is expected.

Analysis of the FTIR spectrum of the MOCN coating also confirms the formation of ZnTPC with notably the rising of the band at 1508 cm^{-1} related to the two methine bridges surrounding the reduced pyrrole (Figure 1f).[26,27] A shift to lower wavenumber of the pyrrole C_β-H deformation band at 790 cm^{-1} is also indicative of chlorin formation.[26] The band at 985 cm^{-1}, assigned to the Zn-N vibration in ZnTPC, confirms the retention of the central metal ion. The significant broadening of the FTIR absorption bands indicates that the formed layer is not composed of discrete ZnTPC molecules, but rather is a mixture of a plurality of ZnTPC arrangements. The relative atomic concentrations, obtained by XPS, of both the evaporated ZnTPP and MOCN coating are found to be rather close to the theoretical one of ZnTPP and ZnTPC (Table S1, Supporting Information). An almost negligible decrease of the zinc element concentration was observed (*i.e.* from 2.0 % to 1.8 % and 1.6 %), while the nitrogen element concentration decreased from 8 % for the theoretical concentration of ZnTPP and ZnTPC to 6 % for the evaporated ZnTPP and 5 % for the MOCN coating. Oxygen, which is not a constituent of

ZnTPP nor ZnTPC, was detected in both the evaporated ZnTPP (*i.e.* 1 %) and MOCN coating (*i.e.* 3 %). The higher oxygen content of the MOCN is consistent with *tert*-butoxy radicals initiating the polymerization of ZnTPP.

To demonstrate the substrate independence, scalability and deposition behavior of the proposed approach, the MOCN coating was deposited onto various substrates. Cross-sectional scanning electron microscopy (SEM) observation of the MOCN coating deposited on trenches on a silicon wafer revealed the non-conformal behavior of the developed approach (**Figure 2**a). The directional nature of the ZnTPP evaporation process undertaken at relatively low vacuum pressure and the high sticking coefficient, due to low substrate temperature (*i.e.* room temperature) in comparison to the ZnTPP crucible temperature (*i.e.* 275°C), are responsible for this non-conformality of the MOCN coating. Non-conformality is especially suitable for the coating of membrane substrates since it promotes the formation of an even coating at their surface, while preventing the detrimental filling of the large porosities that would reduce the overall permeance of the system. Such behavior is illustrated on Figure 2b where a 200 nm MOCN film is deposited onto porous Anodisc alumina membrane (with 200 nm pore size). No MOCN coating is observed inside the pores.

Transmission electron microscopy (TEM) on the MOCN coatings highlights their dense and defect-free structure (Figure 2c-d), no pinhole are observed on the two 50 nm thick MOCN coatings series, either directly deposited onto carbon copper TEM grids (Figure 2c) or delaminated from their glass substrates and further collected on copper TEM grids

(Figure 2d). Such observation was confirmed by atomic force microscopy (AFM) measurements made on a 67 nm thick MOCN coating deposited on a silicon wafer (Figure 2e). More importantly, no grain boundaries can be observed from the high magnification TEM of the MOCN coatings, which stand as dense and amorphous layers. Such structure is particularly suitable for membrane technology, which required the fabrication of defect-free polymer coatings. The proposed CVD approach contrast with previous works based on a RF plasma discharge induced sublimation of porphyrins that were reported to generate highly porous and heterogeneous architectures.[28] The potentiality to deposit the MOCN coatings on large and flexible substrate, *i.e.* PTMSP membrane, is illustrated on Figure 2g. The D-SIMS depth profiling data of a 55 nm thick MOCN coating deposited on a PTMSP membrane suggest that there is no or very limited diffusion of the ZnTPC into the PTMSP substrate (Figure 2f). The intensity gradients of the Zn and N elements, from ZnTPC coating, and of the Si element, from the PTMSP membrane, at the interface between the two materials is most likely due to the surface roughness of the PTMSP membrane. D-SIMS elemental mapping of the MOCN coating on a PTMSP membrane confirmed the full coverage of the substrate. In addition, the combination D-SIMS image of the $^{16}O^{64}Zn$ and $^{12}C^{14}N$ ions mapping suggests a uniform chemical composition of the MOCN coating (Figure S2, Supporting Information).

The capability of depositing the MOCN coatings on flexible PTMSP membranes enabled the investigation of their gas permeation properties. PTMSP is chosen because it is one of the most permeable and rigid polymers.[29] Of note is that permeance data reported in this work are calculated based on the full thickness of the composite membrane, which is the

sum of the PTMSP and MOCN thicknesses. This is in contrast to some other recently reported supported nanomaterial gas separation membranes, where the thickness of the base support layer is excluded from the calculation.[5,30] While the gas permeance of uncoated PTMSP follows the sequence of $CO_2 > H_2 > CH_4 > O_2 > N_2$, which can be ascribed to the combined effects of diffusion and sorption (*e.g.* CO_2 and CH_4 are more condensable), a more remarkable molecular sieving effect was observed for the MOCN coated membrane (**Figure 3**a). In particular, the gas permeances of larger gas molecules (N_2 and CH_4) were significantly depressed, while smaller gas molecules maintained relatively high permeances. Such behaviour is forecasted to lead to large gas separation performances for several important gas pairs, including CO_2/N_2, CO_2/CH_4, O_2/N_2, H_2/N_2 and H_2/CH_4. As shown in Figure 3a, the gas permeance of MOCN films decreased as the thickness of the MOCN layer increased. In contrast, the evaporated ZnTPP layer (*i.e.* non-polymerized) showed rather small reduction in gas permeances when compared with the original PTMSP (Figure 3a and Table S2, Supporting Information), clearly indicating the existence of major defects generated during evaporation. The advantage of MOCN deposition was further confirmed by comparing the gas separation performances of MOCN deposited PTMSP membranes with the pristine and evaporated ZnTPP deposited PTMSP membranes (Figure 3b and Table S2, Supporting Information). Great improvement in the gas selectivity was observed for all five gas pairs of interest. To validate the forecast gas-separation potential of the MOCN films estimated from single gas permeation measurements, the mixed-gas permeation properties of the MOCN films were assessed for the H_2/N_2 gas pair. As indicated in Table S3 (supporting information), the H_2 and N_2 permeances and therefore the resulting H_2/N_2 permeation selectivity, were

highly comparable to the one obtained from the single gas permeation measurements (Table S2, supporting information), fully demonstrating the gas-separation potential of the prepared membranes Additional mixed-gas permeation measurements for other significant gas pairs, i.e., CO_2/N_2, H_2/CH_4, and CO_2/CH_4, under various conditionas arecurrently under investigation. As shown in Table S4 (supporting information), the gas separaton performance of supported MOCN films outperformed those of commercial polymers including polyimide and polysulfone with both higher H_2 and CO_2 permeances and higher related gas selectivities (e.g. H_2/CH_4, CO_2/N_2 and CO_2/CH_4).[31] These gas separation performances are also comparable or even slightly better than those of zeolite[32], and MOF membranes[33], except for some rare cases[34] (Table S4 supporting information).

In addition to potentially superior gas selectivities and permeances, the PTMSP membrane supported MOCN films displayed excellent mechanical robustness against high transmembrane pressure difference (10 bar, higher pressure differences not tested) (Figure S4, Supporting Information). The variation on transmembrane pressure difference (from 1 bar to 10 bar) showed little effect on the gas permeation properties of the supported MOCN films, which differs from the behavior of most of the glassy polymers following dual sorption mode. It is suspected that the rigid backbone and microporous structure of the synthesized MOCN materials resulted in an increase of the diffusion coefficient of the various gas species at higher transmembrane pressure difference, and offset the solubility decrease caused by the pressure increase.[35] Moreover, the accelerated plasticization effect of condensable gases (e.g., CO_2 and CH_4), in the ultrathin MOCN films may also prevent the permeance drop when increase the transmembrane

pressure difference.[36] The superior performance of the supported MOCN films demonstrated in this work should be attractive for practical applications in carbon capture, natural-gas sweetening, air separation, natural-gas purification and hydrogen recovery.

The exact origin of the high gas permeance and high gas selectivity is not clear, however, it is suspected that the existence of micropores within the rigid MOCN structure (associated to a special π stacking arrangement) and the metal sites might be responsible for the gas separation properties of the MOCN coating. In this regard, ellipsometric porosimetry (EP) experiments[37] and density functional theory (DFT) calculation were carried out. Using water (0.27 nm) and toluene (0.60 nm) as probing molecules, EP measurements were performed on MOCN coatings deposited on the silicon wafers (Figure S5, Supporting Information). The vapor sorption isotherms of both of the probing molecules pointed out a microporous structure with a pore volume ratio of *ca.* 0.8 % to 1.7 % (Figure 3c). The pore size, calculated from the Kelvin equation, was as low as 0.4 nm. Nevertheless, if one takes into consideration the observed swelling effect of the water and toluene molecules on the MOCN structure, the real pore size could even be smaller than 0.4 nm, which is comparable to the size of N_2 (0.364 nm) and CH_4 (0.38 nm). Such assumption could potentially explain the steep decrease in the N_2 and CH_4 permeances after the deposition of the MOCN coatings onto the PTMSP membranes. In order to improve our understanding on the MOCN material, geometry optimizations based on density functional theory (DFT) calculations were carried out on a pentameric truncated model (phenyl substituents omitted). The DFT calculated minimum-energy structure reveals a rather rigid aliphatic polymer backbone due to the *trans*-substituted pyrroline heterocycles constituting the backbone (Figure 3d-e). Naturally, the small

pentamer model does not account for chain entanglement or cross-linking but demonstrates the rigidity of the backbone, which is an essential feature of gas separation membranes.[38] In addition, the rigidity of the MOCN porous structure may explain the retained selectivity when increasing the transmembrane pressure (Figure S4, Supporting Information). The zinc chlorin macrocyles are oriented in alternating directions in a stacked manner with Zn···Zn distances of 0.5 to 0.6 nm for the small pentamer model. Such distances could potentially be smaller for the deposited MOCN structure (cross-linked and encumbered by the presence of phenyl-substituents at the *meso*-positions of the macrocycles), which would be consistent with the EP measurements and the observed molecular sieving effect of the MOCN coatings. The microporous and rigid structure of the MOCN coatings (associated to a special π stacking arrangement) might be responsible for the gas separation properties of the MOCN-coated PTMSP membranes. In addition, the presence of the macrocycle metal cation may also contribute to the superior gas separation performance of MOCN coatings and additional experiments involving different central metal cations are currently under investigation.

In conclusion, the CVD polymerization of porphyrin molecular building units has yielded new class of hyper-thin (sub-100 nm), dense and defect-free MOCN coatings. In this first demonstration, and in contrast to many common nanomaterials, the MOCN films were grown directly on thermally sensitive membrane substrates. This new class of films also proved to be mechanically flexible and compatible with operation at the high transmembrane pressures used in commercial gas separation process. Uniform MOCN films over a 150 mm diameter substrate were readily achieved and the well-known

scalability of CVD processes bodes well for fabrication of uniform MOCN layers over even larger lateral dimensions. The nanoporous structure of the MOCN, associated to a π-electron rich environment and to a high density of coordinatively flexible Zn(II) centers is assumed to be at the origin of the gas permeation properties and potentially outstanding gas separation properties of the ultrathin MOCN coating. Further experiments, involving free-base porphyrins and metalloporphyrins are underway in order to determine the influence of the metal cation and assess the gas separation performances of the MOCN coatings. The versatile synthesis approach described in this work is not specific to gas separation and may also pave the way for development of new MOCNs for applications in sensing, catalysis, light-emitting diodes, field-effect transistors and solar cells technologies.

Experimental

Synthesis of the metal organic covalent network coating: MOCN coatings were prepared using iPECVD in a custom-built reactor. The reactor chamber is described in detail elsewhere[39]. Prior to all depositions, the iPECVD chamber was pumped down to a base pressure of less than 1×10^{-4} mbar by mechanical rotary and molecular turbo pumps. For the deposition experiments, argon gas, used as the plasma gas, was flow into the chamber at a flow rate that ensures a constant pressure of 5×10^{-3} mbar in the chamber. Argon flow rates were 10 and 20 sccm for the MOCN coatings and evaporated ZnTPP deposition experiments, respectively. The ZnTPP monomer (PorphyChem, 98 %), used without further purification, was evaporated from a crucible resistively heated at 275 °C and located in the front side of the chamber. The TBPO initiator (Sigma-Aldrich, 98%), used without further purification, was fed into the chamber through a stainless steel line

located in the back side of the chamber. A circular radio frequency (RF) capacitively coupled electrode of outer diameter 14 cm and inner diameter 5 cm was placed 2 cm above the TBPO initiator feeding line outlet situated in the back side of the chamber. The labile peroxide bond of the TBPO initiator was broken by a gentle RF plasma kept at 20 W. RF plasma was generated by an Advanced Energy Cesar RF power generator (Model 136) via a Plasma-Therm RF matching unit (MNS-50CE). The substrates used for the deposition were microscope glass slides, silicon wafers, PTMSP membranes and carbon copper TEM grids placed onto a temperature controlled stage (20 °C) located 15 cm above both the ZnTPP crucible and the RF electrode. For the evaporated ZnTPP thin films, no TBPO initiator was flow to the chamber and RF plasma was not ignited.

Gas permeation experiments: The procedure for single[30, 40] and mixed-gas[41] permeation measurements were similar as described in detail elsewhere. A constant pressure set up was used for both single gas and mixed gas permeation experiments. All gas permeation data were taken after a steady permeation region was reached (Figure S3, Supporting Information).

Acknowledgements

N. D. B. and M. W. contributed equally to this work. N. D. B. is particularly grateful to the Fonds National de la Recherche (FNR) of Luxembourg for supporting his visiting scientist position at MIT (SENSI project). This research was supported by the US Army through the Institute for Soldier Nanotechnologies under Contract DAAD-19-02D-0002 with the US Army Research Office. P. Choquet, N. Valle, B. El Adib, J.-N. Audinot, J. Didierjean, T. Fouquet, G. Frache and N. Desbenoit from LIST are acknowledged for insightful discussions and acquisition of the XPS and mass-spectrometry measurements. We thank D. Borelli, Y. Zhang and N. Watson from MIT for assistance with the iPECVD reactor and the TEM analysis, respectively. Parts of this research were conducted using the supercomputer Mogon and advisory services offered by Johannes Gutenberg

University Mainz (www.hpc.uni-mainz.de), which is a member of the AHRP and the Gauss Alliance e.V.

Received: ((will be filled in by the editorial staff))
Revised: ((will be filled in by the editorial staff))
Published online: ((will be filled in by the editorial staff))

[1] F. Zhang, X. Zou, X. Gao, S. Fan, F. Sun, H. Ren, G. Zhu, *Adv. Funct. Mater.* **2012**, *22*, 3583.

[2] M. Carta, R. Malpass-Evans, M. Croad, Y. Rogan, J. C. Jansen, P. Bernardo, F. Bazzarelli, N. B. McKeown, *Science* **2013**, *339*, 303.

[3] M. Wang, V. Janout, S. L. Regen, *Acc. Chem. Res.* **2013**, *46*, 2743.

[4] Y. Peng, Y. Li, Y. Ban, H. Jin, W. Jiao, X. Liu, W. Yang, *Science* **2014**, *346*, 1356.

[5] H. Li, Z. Song, X. Zhang, Y. Huang, S. Li, Y. Mao, H. J. Ploehn, Y. Bao, M. Yu, *Science* **2013**, *342*, 95.

[6] K. Celebi, J. Buchheim, R. M. Wyss, A. Droudian, P. Gasser, I. Shorubalko, J.-I. Kye, C. Lee, H. G. Park, *Science* **2014**, *344*, 289.

[7] H. W. Kim, H. W. Yoon, S.-M. Yoon, B. M. Yoo, B. K. Ahn, Y. H. Cho, H. J. Shin, H. Yang, U. Paik, S. Kwon, J.-Y. Choi, H. B. Park, *Science* **2013**, *342*, 91.

[8] Q. Song, S. Cao, R. H. Pritchard, B. Ghalei, S. A. Al-Muhtaseb, E. M. Terentjev, A. K. Cheetham, E. Sivaniah, *Nat. Commun.* **2014**, *5*, 4813.

[9] Q. Song, S. Cao, P. Zavala-Rivera, L. Ping Lu, W. Li, Y. Ji, S. A. Al-Muhtaseb, A. K. Cheetham, E. Sivaniah, *Nat. Commun.* **2013**, *4*, 1918.

[10] S. Mathew, A. Yella, P. Gao, R. Humphry-Baker, C. F. E., N. Ashari-Astani, I. Tavernelli, U. Rothlisberger, N. Khaja, M. Grätzel, *Nat. Chem.* **2014**, *6*, 242.

[11] P. Heier, N. D. Boscher, T. Bohn, K. Heinze, P. Choquet, *J. Mater. Chem. A* **2014**,

2, 1560.

[12] P. Heier, N. D. Boscher, P. Choquet, K. Heinze, *Inorg. Chem.* **2014**, *53*, 11086.

[13] M. C. So, S. Jin, H.-J. Son, G. P. Wiederrecht, O. K. Farha, J. T. Hupp, *J. Am. Chem. Soc.* **2013**, *135*, 15698.

[14] Z. Wang, S. Yuan, A. Mason, B. Reprogle, D.-J. Liu, L. Yu, *Macromolecules* **2012**, *45*, 7413.

[15] W. Auwarter, D. Ecija, F. Klappenberger, J. V Barth, *Nat. Chem.* **2015**, *7*, 105.

[16] M. Obata, E. Ohtake, S. Hirohara, M. Tanihara, S. Yano, *J. Polym. Sci. Part A Polym. Chem.* **2012**, *50*, 3592.

[17] A. A. Gridnev, E. M. Nechvolodova, *Theor. Exp. Chem.* **1989**, *25*, 670.

[18] A. M. Coclite, K. K. Gleason, *Plasma Process. Polym.* **2012**, *9*, 425.

[19] C. D. Windle, M. V Câmpian, A.-K. Duhme-Klair, E. A. Gibson, R. N. Perutz, J. Schneider, *Chem. Commun.* **2012**, *48*, 8189.

[20] E. A. Makarova, T. Fukuda, E. A. Luk Yanets, N. Kobayashi, *Chemistry* **2005**, *11*, 1235.

[21] P. Heier, C. Förster, D. Schollmeyer, N. Boscher, P. Choquet, K. Heinze, *Dalton Trans.* **2013**, *42*, 906.

[22] I. Renge, *J. Lumin.* **2013**, *134*, 813.

[23] K. Aravindu, H.-J. Kim, M. Taniguchi, P. L. Dilbeck, J. R. Diers, D. F. Bocian, D. Holten, J. S. Lindsey, *Photochem. Photobiol. Sci.* **2013**, *12*, 2089.

[24] A. D'Urso, M. E. Fragalà, R. Purrello, *Chem. Commun.* **2012**, *48*, 8165.

[25] N. D. Boscher, D. Duday, P. Heier, K. Heinze, F. Hilt, P. Choquet, *Plasma Process. Polym.* **2013**, *10*, 336.

[26] L. L. Gladkov, A. S. Starukhin, A. M. Shul'ga, *J. Appl. Spectrosc.* **1987**, *46*, 154.

[27] L. A. Andersson, T. M. Loehr, R. G. Thompson, S. H. Strauss, *Inorg. Chem.* **1990**, *29*, 2142.

[28] M. Tonezzer, G. Maggioni, E. Dalcanale, *J. Mater. Chem.* **2012**, *22*, 5647.

[29] T. Masuda, E. Isobe, T. Higashimura, K. Takada, *J. Am. Chem. Soc.* **1983**, *105*, 7473.

[30] M. Wang, S. Yi, V. Janout, S. L. Regen, *Chem. Mater.* **2013**, *25*, 3785.

[31] V. Abetz, T. Brinkmann, M. Dijkstra, K. Ebert, D. Fritsch, K. Ohlrogge, D. Paul, K.-V. Peinemann, S. P. Nunes, N. Scharnagl, M. Schossig, *Adv. Eng. Mater.* **2006**, *8*, 328.

[32] J. van den Bergh, W. Zhu, J. Gascon, J. A. Moulijn, F. Kapteijn, *J. Membr. Sci.* **2008**, *316*, 35.

[33] Y. Liu, G. Zeng, Y. Pan, Z. Lai, *J. Membr. Sci.* **2011**, *379*, 46.

[34] Y. Peng, Y. Li, Y. Ban, H. Jin, W. Jiao, X. Liu, W. Yang, *Science* **2014**, *346*, 1356.

[35] P. Li, T. S. Chung, D. R. Paul, *J. Membr. Sci.* **2013**, *432*, 50.

[36] M. Wessling, M. L. Lopez, H. Strathmann, *Sep. Purif. Technol.* **2001**, *24*, 223.

[37] A. Perrotta, E. R. J. van Beekum, G. Aresta, A. Jagia, W. Keuning, R. M. C. M. van de Sanden, E. W. M. M. Kessels, M. Creatore, *Microporous Mesoporous Mater.* **2014**, *188*, 163.

[38] M. D. Guiver, Y. M. Lee, *Science* **2013**, *339*, 284.

[39] D. C. Borrelli, S. Lee, K. K. Gleason, *J. Mater. Chem. C* **2014**, *2*, 7223.

[40] M. Wang, V. Janout, S. L. Regen, *Langmuir* **2010**, *26*, 12988.

[41] H. Guo, G. Zhu, I. J. Hewitt, S. Qiu, *J. Am. Chem. Soc.* **2009**, *131*, 1646.

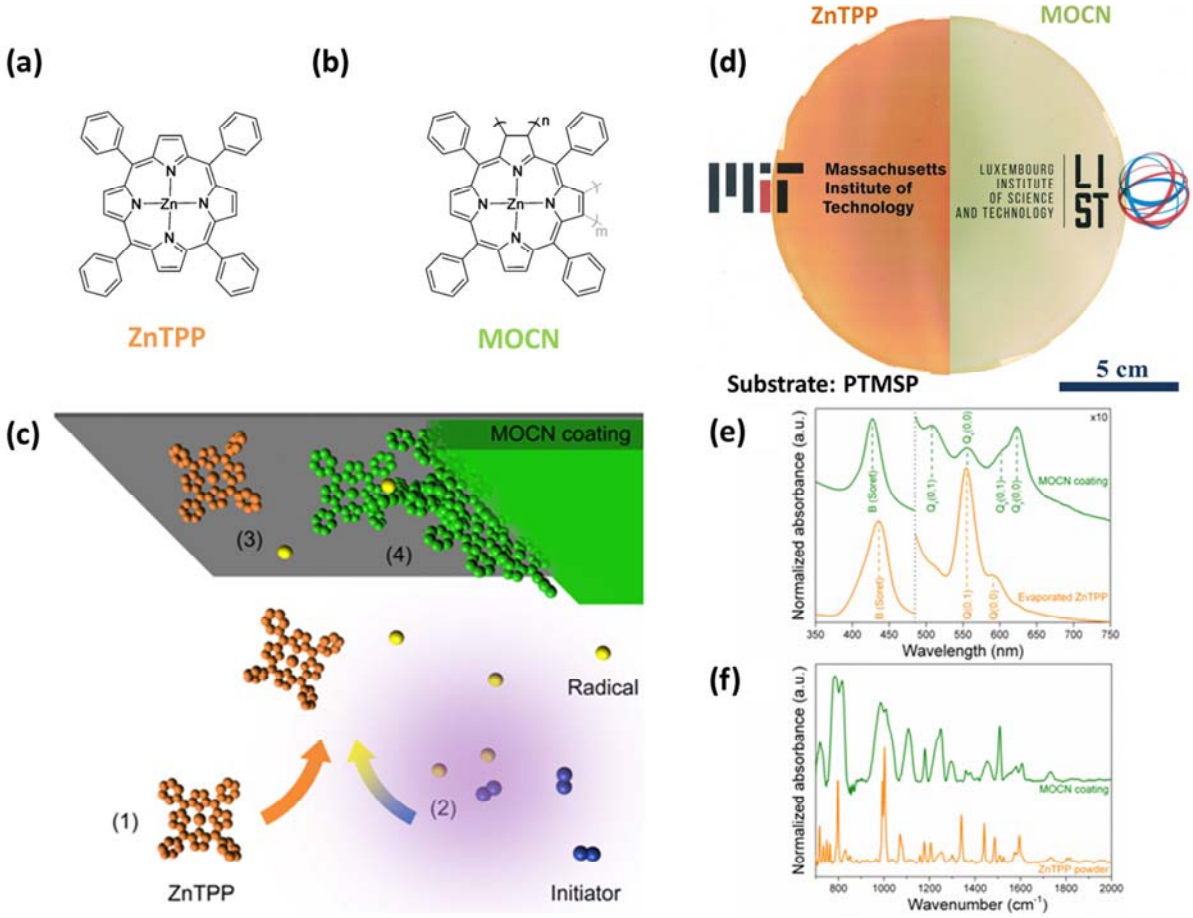

Figure 1. Synthesis of the porous MOCN coating. a) Molecular structure of zinc (II) *meso*-tetraphenylporphyrin (ZnTPP) investigated as the building unit of the MOCN coating. b) Proposed molecular structure of metal organic covalent network (MOCN). The second reduced *exo*-pyrrole double bond in grey is expressing the possible formation of a small amount of zinc (II) *meso*-tetraphenylisobacteriochlorin that cannot be ruled out. c) Schematic of the iPECVD process mechanism: (1) vaporized ZnTPP monomer is introduced, (2) vaporized TBPO initiator is introduced and dissociated into radicals by exposure to a plasma discharge positioned away from the substrate, (3) the monomer and initiator radicals are adsorbed onto the surface of the substrate (20 °C), (4) where they undergo free-radical polymerization to form a MOCN coating. d) Optical image of evaporated ZnTPP (left) and the MOCN coating (right) on the poly[1-(trimethylsilyl)-1-

propyne] (PTMSP) membrane. e) UV-vis absorption spectra of the evaporated ZnTPP (below) and the MOCN coating (above). f) ATR-FTIR absorption spectra (only the range between 700 and 2000 cm^{-1} is shown) of the monomer (ZnTPP) powder (below) and of the MOCN coating (above).

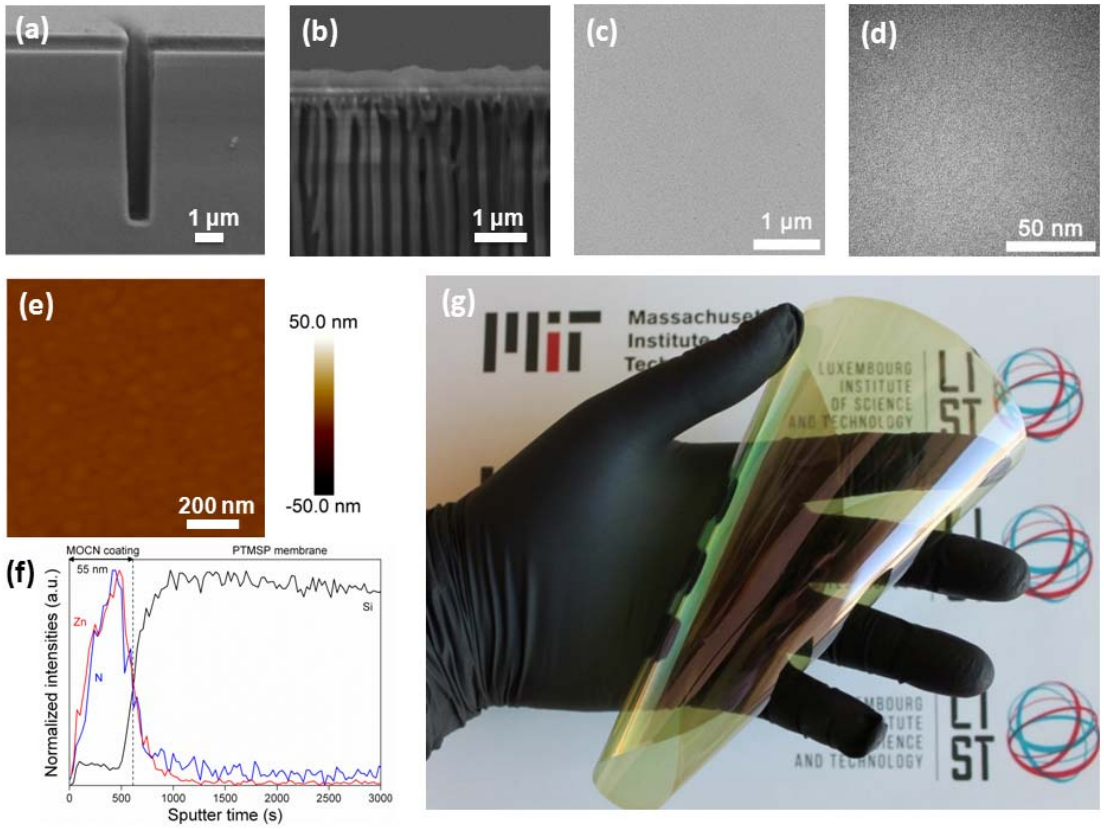

Figure 2. Characterisation of the metal organic covalent network (MOCN) coating. a) Cross-sectional scanning electron microscopy (SEM) image of a 200 nm thick MOCN film deposited on a 600nm × 5mm silicon trenched wafer. b) Cross-sectional SEM image of a 200 nm thick MOCN film deposited on porous Anodisc alumina membrane with 200 nm pores. c) Low magnification TEM image of a MOCN coating directly deposited in-situ onto a carbon copper TEM grid. d) High magnification TEM image of a MOCN coating collected onto a copper TEM grid. e) Atomic force microscopy (AFM) image of MOCN coated silicon wafer with root mean square (RMS) roughness of 0.6 nm. f) Zn, N and Si D-SIMS depth profiles for a 55 nm thick MOCN coating on a PTMSP membrane. g) Optical image of flexed MOCN coated, large-area, PTMSP membrane.

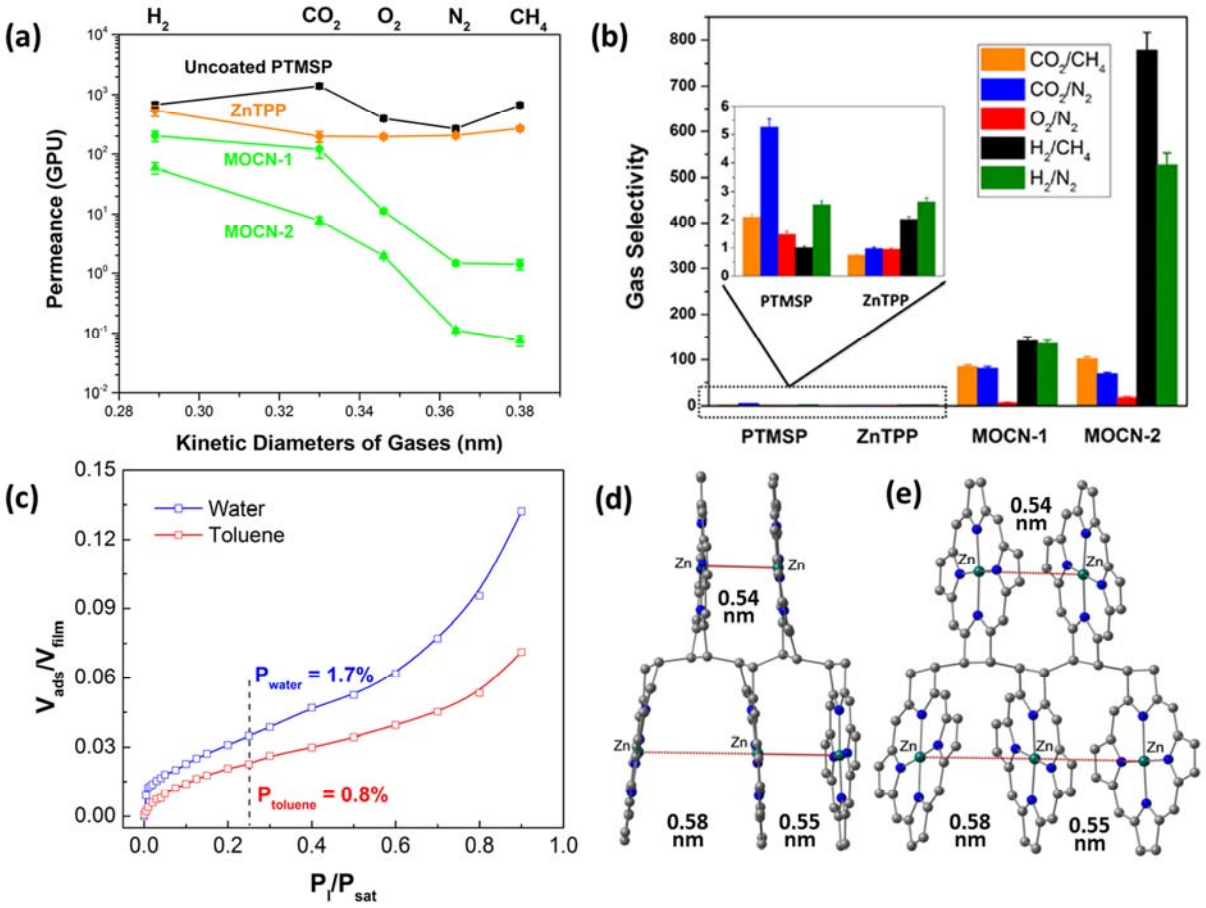
(a)
H2
CO2
O2
N2
CH4
Uncoated PTMSP
ZnTPP
MOCN-1
MOCN-2
Permeance (GPU)
Kinetic Diameters of Gases (nm)
(b)
CO2/CH4
CO2/N2
O2/N2
H2/CH4
H2/N2
Gas Selectivity
PTMSP
ZnTPP
MOCN-1
MOCN-2
(c)
Water
Toluene
Vads/Vfilm
Pwater = 1.7%
Ptoluene = 0.8%
Pl/Psat
(d)
Zn
0.54 nm
0.58 nm
0.55 nm
(e)
0.54 nm
0.58 nm
0.55 nm

Figure 3. Gas sorption and transport properties. a) Gas permeances of membranes as a function of kinetic diameters of different gases. Black filled square: untreated PTMSP; Orange filled diamond: evaporated ZnTPP coated PTMSP membrane; Green filled circle: MOCN-1 coated PTMSP membrane (47nm); Green filled triangle: MOCN-2 coated PTMSP membrane (67 nm). b) Gas selectivity of untreated PTMSP, evaporated ZnTPP and MOCN treated PTMSP. Orange bar: CO_2/CH_4, blue bar: CO_2/N_2, red bar: O_2/N_2, black bar: H_2/CH_4 and olive bar: H_2/N_2. The inset is a magnified display of the gas selectivity of PTMSP and evaporated ZnTPP treated PTMSP. c) Adsorption/desorption isotherms measured by ellipsometric porosimetry, using water vapor (kinetic diameter, 0.27 nm) and toluene vapor (kinetic diameter, 0.60 nm) molecules as probing molecules. d) & e) DFT (BP, def2-SV(P)) optimized geometry of a pentamer model with truncated phenyl substituents (H atoms omitted for clarity).

The chemical vapor deposition (CVD) polymerization of metalloporphyrin building units is demonstrated to provide an easily up-scalable one-step method towards the deposition of new class of dense and defect-free metal organic covalent network (MOCN) layers. The resulting hyper-thin and flexible MOCN layers do exhibit outstanding gas separation performances for multiple gas pairs.

Metalloporphyrins; iPECVD; Free-radical polymerization; Metal organic covalent network; Gas separation

N. D. Boscher, M. Wang, A. Perrotta, K. Heinze, M. Creatore, K. K. Gleason*

Metal organic covalent network chemical vapor deposition for gas separation